Cell Reports

Article

Plaque contact and unimpaired *Trem2* is required for the microglial response to amyloid pathology

Graphical abstract

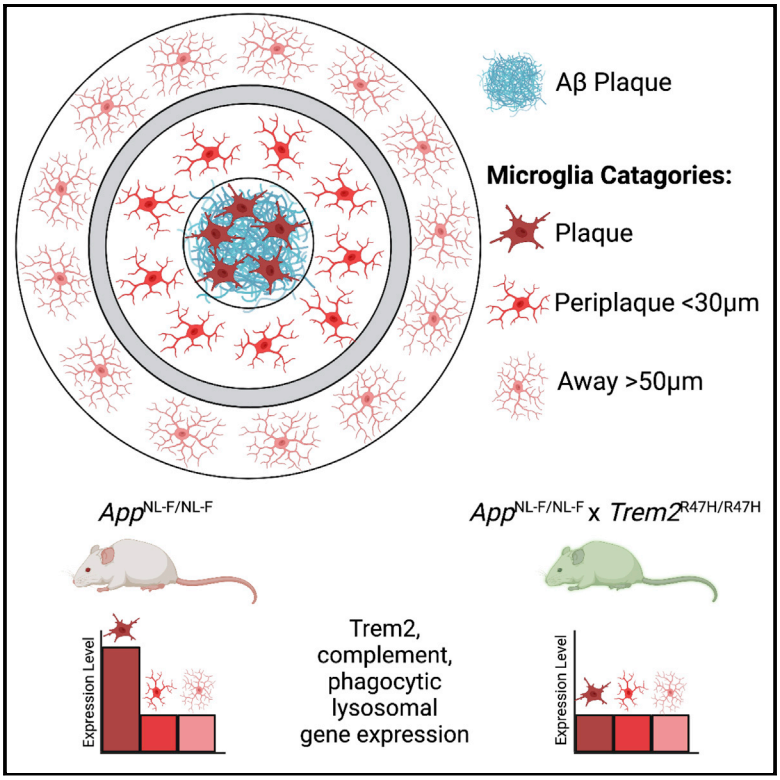

Highlights

- Microglial-enriched spatial transcriptomics reveals effects of plaque contact
- *Trem2* among genes only increases in microglia on plaques in *App*$^{NLF/NLF}$ (NLF) mice
- No increased expression of *Trem2* and a small gene module in *NLFTrem2*$^{R47H/R47H}$ mice
- *Trem2* module includes: complement *C1qa,c;* phagosome *Plek*, *Cd68*,; lysosome *Ctss*, *Ctsz*, *Grn*

Authors

Jack I. Wood, Eugenia Wong, Ridwaan Joghee, ..., Damian M. Cummings, John Hardy, Frances A. Edwards

Correspondence

f.a.edwards@ucl.ac.uk

In brief

Wood et al. use spatial gene expression analysis to assess the effect of microglia plaque contact in aged *App* knockin mice. Genes in a pathway from *Trem2,* complement factors, phagocytosis, and lysosomal degradation have increased expression in microglia on plaques; increased expression is prevented with human GWAS risk mutation *Trem2*^{R47H}.

Wood et al., 2022, Cell Reports *41*, 111686
November 22, 2022
https://doi.org/10.1016/j.celrep.2022.111686

CellPress

Cell Reports

CellPress
OPEN ACCESS

Article

Plaque contact and unimpaired *Trem2* is required for the microglial response to amyloid pathology

Jack I. Wood,[1,5] Eugenia Wong,[1] Ridwaan Joghee,[1] Aya Balbaa,[1] Karina S. Vitanova,[1] Katie M. Stringer,[1,5] Alison Vanshoiack,[2] Stefan-Laural J. Phelan,[2] Francesca Launchbury,[3] Sneha Desai,[1] Takshashila Tripathi,[1] Jörg Hanrieder,[3,5] Damian M. Cummings,[1] John Hardy,[4,3] and Frances A. Edwards[1,6,7,*]

[1]Department of Neuroscience, Physiology & Pharmacology, University College London, Gower Street, London WC1E 6BT, UK
[2]Nanostring Technologies, 530 Fairview Avenue N, Seattle, WA 98109, United States
[3]Department of Neurodegenerative Disease, University College London Queen Square Institute of Neurology, Queen Square, London WC1N 3BG, UK
[4]Dementia Research Institute, University College London, Gower Street, London WC1E 6BT, UK
[5]Department of Psychiatry and Neurochemistry, Institute of Neuroscience and Physiology, Sahlgrenska Academy at the University of Gothenburg, Mölndal Hospital, House V3, 43180 Mölndal, Sweden
[6]Institute of Healthy Ageing, University College London, Gower Street, London WC1E 6BT, UK
[7]Lead contact
*Correspondence: f.a.edwards@ucl.ac.uk
https://doi.org/10.1016/j.celrep.2022.111686

SUMMARY

Using spatial cell-type-enriched transcriptomics, we compare plaque-induced gene (PIG) expression in microglia-touching plaques, neighboring plaques, and far from plaques in an aged Alzheimer's mouse model with late plaque development. In 18-month-old $APP^{NL\text{-}F/NL\text{-}F}$ knockin mice, with and without the Alzheimer's disease risk mutation $Trem2^{R47H/R47H}$, we report that expression of 38/55 PIGs have plaque-induced microglial upregulation, with a subset only upregulating in microglia directly contacting plaques. For seven PIGs, including *Trem2*, this upregulation is prevented in $APP^{NL\text{-}F/NL\text{-}F}Trem2^{R47H/R47H}$ mice. These TREM2-dependent genes are all involved in phagocytic and degradative processes that we show correspond to a decrease in phagocytic markers and an increase in the density of small plaques in *Trem2*-mutated mice. Furthermore, despite the R47H mutation preventing increased *Trem2* gene expression, TREM2 protein levels and microglial density are still marginally increased on plaques. Hence, both microglial contact with plaques and functioning TREM2 are necessary for microglia to respond appropriately to amyloid pathology.

INTRODUCTION

The importance of the microglial membrane receptor TREM2 in Alzheimer's disease (AD) is now well known. The initial evidence came from genome-wide association studies (GWAS), which convincingly demonstrated that *TREM2* has several variants that increase the risk of reaching the stage of AD diagnosis. $TREM2^{R47H}$, the most common risk variant, has an effect size similar to that of the *APOE4* allele in people of White European descent.[1–3] Considerable work has been undertaken using mouse models carrying familial AD mutations, *Trem2* knockout mice, and primary microglial cultures,[4] reviewed in Gratuze et al. and Kulkarni et al.,[3,5] revealing that TREM2 pushes microglia away from an inflammatory cytokine-producing phenotype toward an anti-inflammatory phagocytic phenotype[4] and has been reported to be instrumental in the increased density of microglia around plaques. Moreover, microarray analysis of transgenic mice, carrying familial AD mutations, revealed *Trem2* and an array of co-expressed genes to be upregulated in the hippocampus and cortex,[6] a finding repeatedly confirmed with RNA-seq, both in whole tissue[7] and in single-cell studies. Such single-cell RNA-seq studies have confirmed patterns of gene expression defining "disease-associated microglia" (DAM) genes[8] in relation to amyloidβ (Aβ)[9] and Tau pathology.[10] A recent study using spatial transcriptomics in relation to plaque density defined a further overlapping group of genes referred to as plaque-induced genes, PIGs.[11]

Most of the mouse studies published have focused on transgenic mice that overexpress familial AD mutations in *App* and/or *Psen1* or *Psen2* genes. Moreover, when knockin mice are used, the most popular model has been the $App^{NL-G-F/NL-G-F}$ (NLGF) mouse,[12] which harbors three familial AD mutations in *App* and includes a humanized Aβ sequence. Similarly to transgenic models, NLGF mice deposit plaques rapidly and early, such that the most rapid increase in plaque load occurs between 2 and 4 months of age, reaching almost maximal density by 9 months.[13] Sporadic AD develops slowly from midlife into old age, so the reaction of microglia to this rapid rise of plaques in

young animals may be very different and less relevant than their response to slow deposition starting later in life. A further difference is that the inclusion of the Arctic mutation in the NLGF mouse within the Aβ sequence results in a more fibrillar form of Aβ causing rapid deposition and probably lower levels of soluble Aβ in the neuropil. Consequently, we suggest that the $App^{NL-F/NL-F}$ (NLF) mouse[12] is a better model of sporadic AD than the NLGF mouse as, in NLF mice, the Aβ sequence is the same as in the sporadic disease, and the plaques begin to develop slowly in midlife and increase through to at least 24 months of age. Although using these very old mice is inconvenient and increases the cost of studies, the increased relevance of combining slow development and, importantly, the element of old age outweighs these disadvantages. However, until recently, analyzing changes in gene expression was very difficult in NLF mice because, even at 24 months of age, genes such as *Trem2* show only modest changes, despite evident synaptic differences and increased microglial density.[13] It is this combination of high cost and low reward that has made NLFs a less popular model, despite the similarity to the progression of human sporadic AD. However, with the introduction of spatial cell-type-enriched transcriptomics, more subtle and direct analysis of plaque-induced microglial gene expression changes becomes possible, without the diluting effects of bulk analysis.

Using spatial transcriptomics in this more relevant mouse model, we initially compare microglial-enriched expression of PIGs. PIGs were defined by Chen et al. (2020)[11] in NLGF mice as genes that upregulate in response to plaque density in different brain regions and across multiple cell types. For more than half of these genes, we confirm, in NLF mice, that association with plaque increases expression. Importantly, in a subset of these genes, this only occurs in microglia directly in contact with plaques and not in immediately neighboring regions.

We particularly study *Trem2* as one of the genes upregulated specifically on plaques in these mice. We compared the effects in NLF mice to NLF mice in which $Trem2^{R47H/R47H}$ is knocked in ($NLFTrem2^{R47H}$ double homozygous mice) and validated our findings at the protein level using immunohistochemistry. The lack of *Trem2* upregulation in the $NLFTrem2^{R47H}$ mice could then be used to assess whether increased microglial density at plaques depends on *Trem2* genotype. Surprisingly, in $NLFTrem2^{R47H}$ mice, the density of microglia increased considerably, which may be due to a modest increase in TREM2 protein expression, in the absence of increased gene expression.

RESULTS

In NLF mice, plaques are first detected at 9 to 10 months of age. Deposition then slowly increases through to 24 months of age.[13] In the present study, we investigate the spatial distribution of gene expression in 18-month-old NLF and $NLFTrem2^{R47H}$ mice.

For spatial transcriptomics analysis, we labeled plaque pathology and associated glial cells using immunohistochemistry toward TMEM119 (microglia), GFAP (astrocytes), and Aβ40/Aβ42 (plaques) (Figure 1A). We then selected large regions of interest (ROIs) that were densely filled with plaques and nearby ROIs without plaques (Figures 1Bi and 1Bii). Most plaques in the hippocampus of the NLF mouse hippocampal sections used in this study were found in and around the *stratum lacunosum moleculare* of CA1–3 and the *stratum moleculare* of the dentate gyrus (Figure 1Bii). It is thus possible, in each brain section, to define ROIs in which all pixels are within ~30 μm of a plaque and other ROIs in which no plaques are detected. We then defined cell-type-enriched areas of interest (AOIs) for microglia or astrocytes within each ROI. For the present study, we focused on microglia and determined genome-wide RNA signatures from the following three types of AOIs in NLF and $NLFTrem2^{R47H}$ mice: (1) "on plaque," all the microglia in the plaque ROIs that colocalized with Aβ (Figure 1Ci); (2) "periplaque," all the microglia in the plaque ROI that did not colocalize with Aβ (Figure 1Cii); and (3) "away" from plaque, all the microglia in the ROIs without plaques. In addition, ROIs in equivalent positions were studied in wild-type (WT) and $Trem2^{R47H}$ mice, so that the same regions could be compared without plaques. Before collecting RNA signatures from the microglial AOIs, signatures were collected from the regions labeled with the GFAP antibody in order to decrease contamination from overlapping astrocytes. However, it is important to note that the results represent enrichment for microglia rather than selective analysis of microglial genes. Indeed, some highly expressed genes from astrocytes and neurons are also detected in the microglial gene set. Nevertheless, a useful degree of separation between cell types is achieved, as can be seen when comparing the expression of genes previously defined as microglia enriched[14,15] (Figure S1A) and in principal components analysis (Figure S1B). Note that although TMEM119 has been previously reported to decrease in expression in DAM microglia,[9,16] using immunohistochemistry, we found no change in signal intensity at plaque when compared with 50 μm away (Figure S2).

Note that standard analysis methods for gene expression have mostly been developed for analysis of postmortem human tissue. This requires complex normalization methods to overcome the problems of heterogeneity in the genetic and environmental background of the subjects, condition of the tissue, cause of death, postmortem interval, and other variables, depending on the source of the tissue. The situation is completely different in mice that have identical genetic backgrounds (except for the genes altered for the experiment) and controlled conditions for environment, diet, killing of the animal, treatment of the tissue, and extraction methods. Consequently, much simpler methods of normalization are sufficient, such as using housekeeping (HK) genes. As this study is concentrating on the microglial AOIs, all data were normalized to *Actg1* and *Actb*. To verify this method, we compared HK normalization with the more standardly used edgeR-based TMM-weighted normalization[17] or Q3 normalization. Comparing the AOI counts normalized with these three methods results in a very high correlation in each case ($r > 0.95$; $p < 0.0001$).

The data for all PIG genes are available at https://edwardslab.shinyapps.io/MouseacST/.

Density of microglia around plaques does not influence analysis of gene expression

As has frequently been reported, microglia cluster around plaques in both mouse models and human tissue.[6,18,19] This is also true in NLF mice, where we have reported that an overall

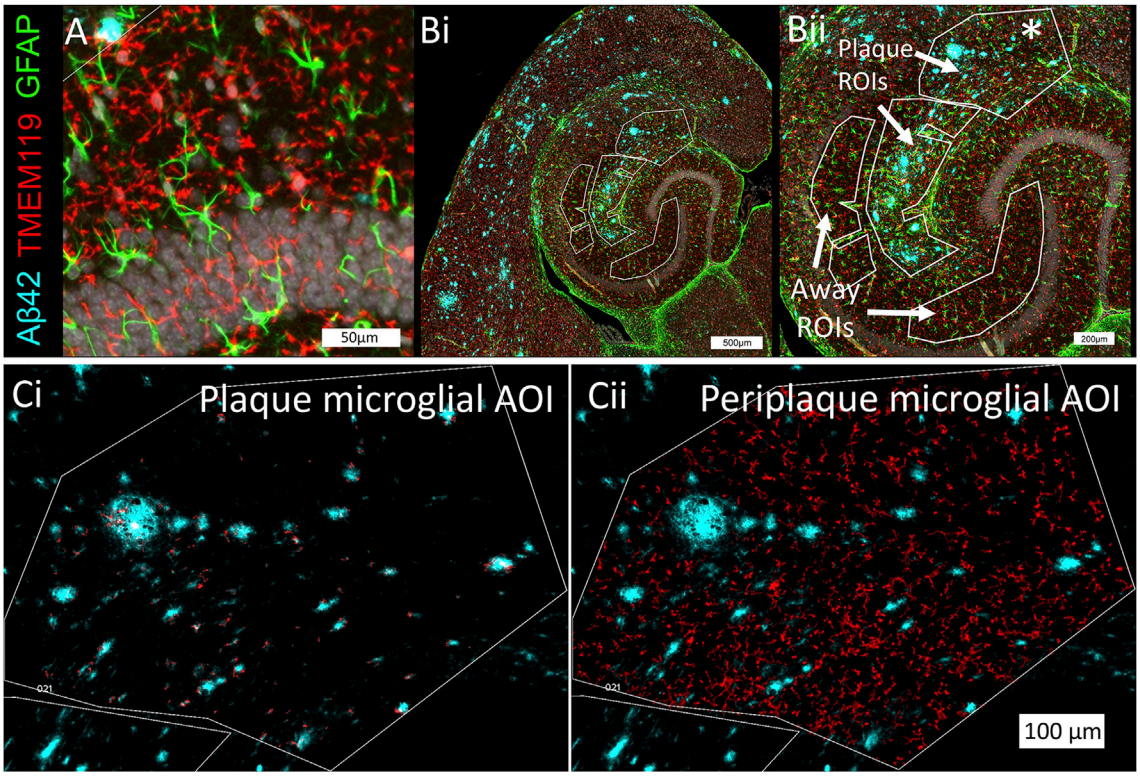

Figure 1. Selection of areas of interest (AOIs)

Sections of the hippocampus and neighboring cortex (8 μm thick) were mounted and labeled with antibodies for plaques (cyan, Aβ40/Aβ42), microglia (red, TMEM119), astrocytes (green, GFAP), and nuclei to reveal the cell bodies of the hippocampus (white, DAPI).

(A) Example image: microglia (red) and astrocytes (green) could be readily identified. A small plaque is visible in the top-left corner (cyan), and a section of the dentate gyrus granule cell body layer is visible in white.

(B) Regions of interest were established that either contained a heavy plaque load (Plaque ROI) or lacked plaques (Away ROI). Bii shows a zoomed in image of the hippocampal region of the full section shown in Bi. * indicates the ROI detailed in (C).

(C) To maximize the separation of microglia, the samples from astrocytes (GFAP-labeled areas) were first removed before collecting from the microglia regions. The plaque ROIs were then separated into subareas of interest (AOIs) whereby the plaque microglial AOI was defined as TMEM119-positive cells that colocalized with Aβ42 (Ci), and periplaque were all TMEM119-labeled cells that did not colocalize with Aβ42 (Cii).

increase in microglial density across the hippocampus of NLF mice only reaches statistical significance at 24 months.[13] In order to ensure that any change in gene expression in our spatial transcriptomics analysis was adequately corrected by the normalization procedure, we checked that expression was not substantially affected by differences in microglial density but truly reflected gene expression per microglial cell. We thus compared the distribution of microglia around individual plaques by comparing the density of IBA1-positive cells (Figures 2A and 2B) to the expression of the microglial gene *Aif1* that codes for IBA1 (Figure 2C). The expression of *Aif1* in individual microglial cells would not be expected to increase substantially in response to plaques. As expected, when density of microglia was assessed on plaques and in concentric circles increasing by 10-μm radius out from the plaque edge, there was a substantial increase in density in the proximity of plaques. However, the increase in microglial density was only detectable at the plaque or within the first 10-μm ring around the plaque. By 20 μm, the density had returned to the level far from plaques, which was also not significantly different from the density in WT mice. Despite the >30-fold increase in density of microglia at the plaque, no significant effect of region or genotype was detected in *Aif1* expression. Other microglial genes not affected by the vicinity to plaques include *Tmem119* and *P2y12.*

It should be noted that for all immunohistochemistry experiments, the plaque has been labeled with luminescent conjugated oligothiophenes (LCOs, "Amytracker"). Use of LCOs will define only deposited Aβ[20–22] and so is rather more stringent in terms of defining the plaque than the Aβ42 antibody used for the transcriptomics, above which may label more diffuse Aβ around the plaque.

Most, but not all, previously defined plaque-induced genes, including *Trem2*, show significant differences between microglia on plaques and far from plaques

As a first step in comparing the regional expression of relevant genes in relation to the position of plaques, we compared the microglial-enriched expression of the genes previously defined as PIGs[11] (Figures 3A–3C).

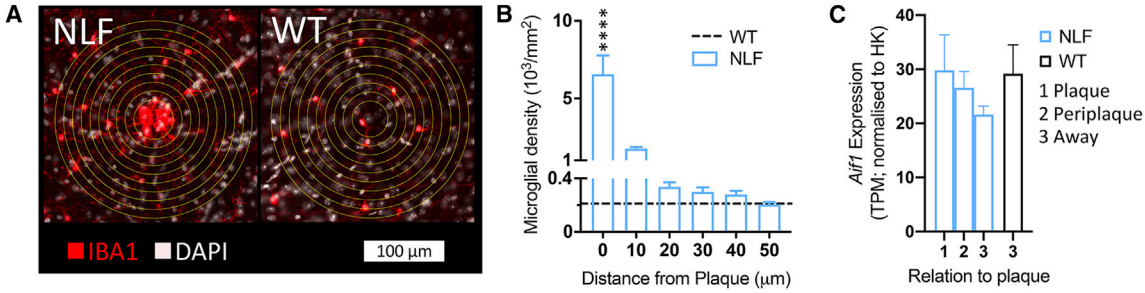

Figure 2. Microglial density compared with *Aif1* expression

(A) Microglia were labeled with an antibody against IBA1 (red), plaques with LCOs (not shown), and nuclei with DAPI (white). For NLF mice, a circle was drawn around the circumference of the plaque, and concentric circles were drawn around this central ring with radii increasing by 10 μm. Microglia were counted in the inner circle and each circle of increasing size. A microglial cell touching a circle was considered to lie inside that circle, and density was calculated. For WT mice, a central circle with a 10-μm radius was placed pseudo-randomly to represent similar areas to those assessed in the NLF mice. Microglial density was counted as for NLF mice.

(B) Quantification of microglial density in NLF mice reveals a 30-fold higher density on the plaque compared with WT mice; one-way repeated measures ANOVA: main effect of distance, $p < 0.0001$.

(C) the expression of *Aif1* (which encodes IBA1) in NLF mice was not significantly increased either compared with WT mice or with distance from plaque. Data are expressed as mean + SEM. n = 6 mice per genotype in (B), and n = 6 NLF, n = 4 WT mice in (C).

Of the 55 tested PIGs, expression of 38 genes showed a significant main effect of relation to plaque in the microglial AOIs (one-way ANOVA). (Two pseudogenes reported as PIGs [*Gpx4-ps* and *Cd63-ps*] were not available in the Nanostring platform.) We divided the differentially expressed genes into three groups: (1) genes only significantly raised in microglia touching plaques (Figure 3A), (2) genes with expression that decreased gradually with the plaque region showing significantly higher expression than the away region but the periplaque region not differing significantly from either, or differing significantly from both (Figure 3B), and (3) genes that were not different between plaque and periplaque but significantly upregulated in both the plaque and periplaque region compared with the away AOIs (Figure 3C). Two additional PIG genes (*H2-k1* and *Ctsh*) were also of interest as they appeared to have a U-shaped response to plaque proximity, being significantly increased in the periplaque area but returning to background levels of expression on the plaque (data not shown). This could suggest an effect on expression of these genes of low concentrations of soluble Aβ in the periplaque region that was lost at higher concentrations near the plaque.

Group 1 was of particular interest, as these genes are most likely responding to contact with the plaque itself, rather than to soluble Aβ or other secreted substances at a distance from the plaque. This group included *Trem2* and its downstream signaling partner *Tyrobp,* as well as several of the complement and lysosomal genes that have previously been implicated in AD.

Note that not all PIGs are thought to be microglial genes. We thus compared the different groups in terms of previously defined relative distribution in microglia or astrocytes in single-cell transcriptomic analysis comparing specific cell types.[14] Figure 3D indicates the proportion of genes in each group that have been reported to be at least 2-fold enriched for microglia or astrocytes compared with all other cell types in whole brain. Genes that were not defined as astrocytic or microglial in the Ximerakis et al. database were further assessed using RNA-seq data of cortical expression in young mice, https://www.brainrnaseq.org.[15] Interestingly, all genes in group 1 and group 2, except *Cd9* and *Gfap* respectively, have been reported to be highly enriched in microglia. Although, it should be noted that *Cd9* has been reported to be upregulated in disease-state microglia.[9] In contrast, the genes in group 3 were all reported to be enriched in astrocytes. Thus, the signal in the microglial AOIs that is likely coming from a remaining overlap of astrocytic processes is seen equally in the plaque and periplaque regions but occurs somewhat less in the region away from plaques. This probably reflects astrogliosis in the plaque ROIs relative to the ROIs without plaques. As shown by immunohistochemistry of GFAP-labeled astrocytes, astrogliosis only decreases slightly in the periplaque regions (10–50 μm; Figure S3), unlike the on-plaque specificity of microglial density (Figure 2).

TREM2 levels in the tested regions are only slightly decreased in the Trem2^{R47H} mice compared with WT

We were particularly interested in *Trem2*, which has consistently appeared as a hub gene in our analysis and that of other groups.[6,7,9,11,23] In the present study, *Trem2* was among the PIGs that only increased in expression in microglia if they were touching plaques (group1, Figure 3A). To investigate the effect of decreasing efficacy of TREM2, the NLF mice were crossed with Trem2^{R47H} knockin mice from Jackson Laboratories, with mice being bred to homozygosity for both the *App^{NL-F}* and the *Trem2^{R47H}* mutations (NLFTrem2^{R47H} mice). It has previously been reported that the Jackson Laboratories Trem2^{R47H} KI mice show a substantial decrease in *Trem2* expression in young mice to about 50% compared with WT mice and an even greater loss of protein in both whole brain or whole hippocampus.[4,23,24] We thus initially considered this to be a study of decreasing the effect of TREM2 both due to decreased TREM2 level and the effect of the loss-of-function R47H AD risk mutation. Moreover, in the whole hippocampus in age- and genotype-matched mice from our colony, we confirmed a substantial reduction (63%) in *Trem2* expression in the Trem2^{R47H} mice compared with WT using RT-qPCR (Figure S4B).

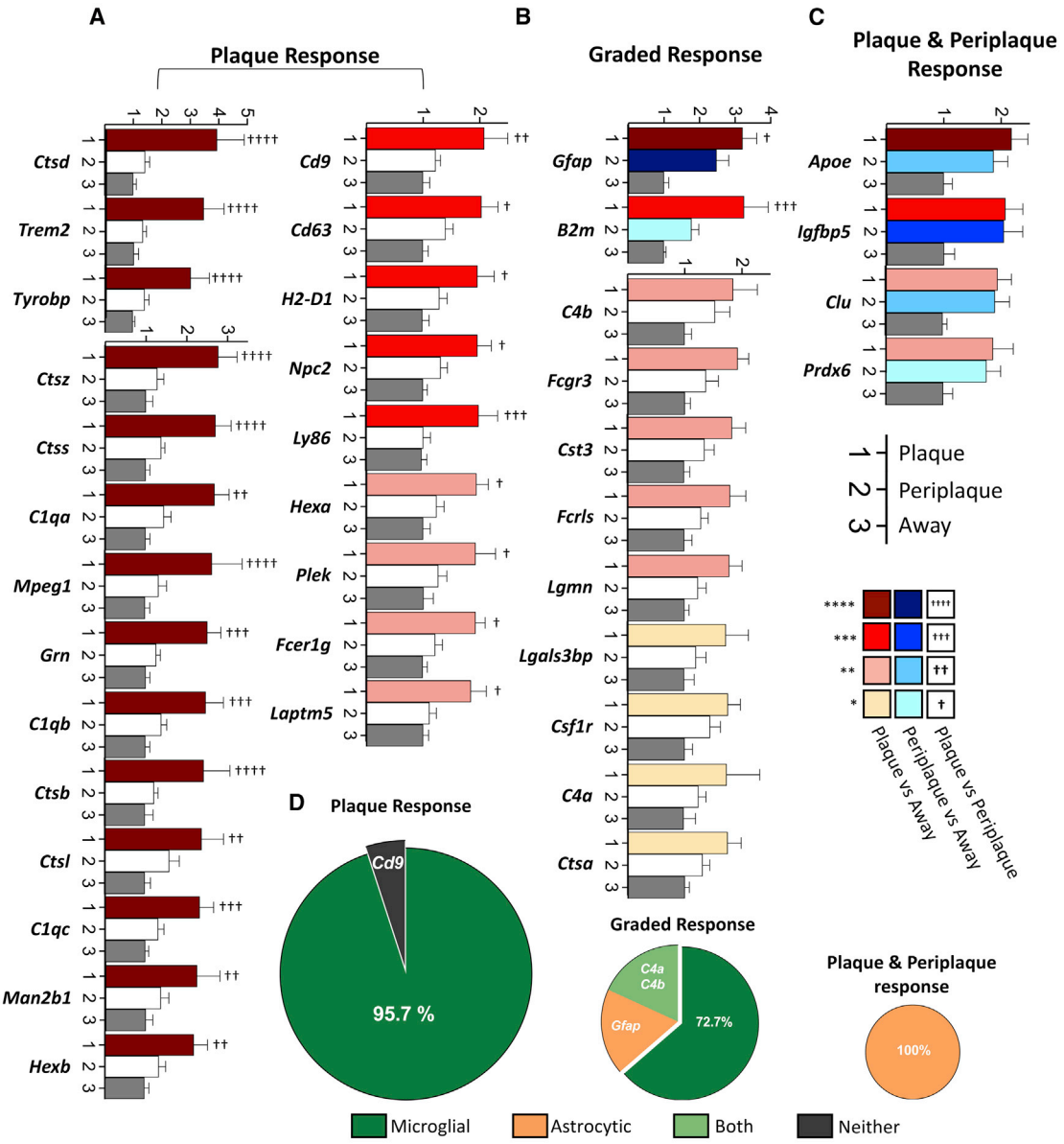

Figure 3. Expression of PIGs in relation to plaques in NLF mice

38 of the 55 PIGs tested in NLF mice show significant main effect of relation to plaque in a two-way repeated measures ANOVA; bar color and dagger symbol represent the result of Tukey *post hoc* correction for multiple comparisons between relation to plaque and gene.

(A) 23 genes were only upregulated when microglia are touching plaques.

(B) 11 genes show a graded response in which expression gradually increases from away through to plaque regions.

(C) Four genes are equally upregulated in the plaque and periplaque regions, both with increased expression compared with away. For other PIGs, there was no significant effect of relation to plaque (not shown). Data are presented as mean + SEM; n = 6 mice. Transcripts were averaged from one to three AOI per mouse. Y axis is fold change compared with the away region.

(D) Pie charts illustrating the percentage of genes that are identified as microglial (green), astrocytic (orange), both (light green), or neither (gray). Cell specificity was assessed according to comparative single-cell RNA-seq analysis from wild-type mice whole brain[14] or cortex Barres Brain RNA-seq database.[15] Genes were considered specific to microglia or astrocytes if expressed ≥ 2-fold compared with all other tested cell types. n = 6 mice. Statistical difference as indicated ****/††††$p < 0.0001$; ***/†††$p < 0.001$; **/††$p < 0.01$; */†$p < 0.05$.

However, in the spatial transcriptomics data from aged mice, the difference, if any, was considerably less. The Trem2^{R47H} mice showed a non-significant mean reduction in expression of *Trem2* of about 20% compared with WT ($p = 0.24$, Figure S4A). Moreover, this trend of a 20% reduction was also reflected in the protein levels as confirmed using immunohistochemistry, which showed a significant 24% reduction in TREM2 ($p < 0.01$; mean TREM2 intensity in IBA1-positivie pixels, Figure S4Ci). It should

be noted that, rather than representing whole hippocampus, the sections for the transcriptomics study were taken from central hippocampus and toward the more dorsal region to obtain sections that were transverse to the dorsal-ventral axis of the hippocampus. Moreover, the AOIs mimicked those for the NLF mice, thus avoiding the cell body layers of the hippocampus, sampling primarily in the apical dendritic regions of the CA1 and CA3 neurons. As the spatial transcriptomics and immunohistochemistry results agreed, this suggests either a technical artifact in the RT-qPCR or a difference dependent on the region of hippocampus tested. Unfortunately, further aged mice were not available for assessment of differential expression between the dorsal and ventral hippocampus. However, immunohistochemical analysis of the whole fixed dorsal hippocampal sections and also different regions within the sections did not reveal any significant differences (Figure S4Cii) from our original immunohistochemical analysis.

In terms of technical differences, RT-qPCR would be expected to show a greater signal to noise ratio than the other methods used, especially in isolated microglia as used by Xiang et al. (2018),[24] but this would only affect genes with very low expression. The strong signal for *Trem2* would not have been measurably influenced by the nonspecific binding (as measured using negative probes), as this was too low for detection. We cannot discount the possibility that other artifacts of the binding of probes to the *Trem2*^{R47H} sequence of one or both of the alternative variants produced decreases the signal for the PCR analysis but is picked up by the transcriptomics probe. However, substantial molecular differences have been reported to occur along the dorsal-ventral hippocampal axis,[25] and we hypothesize that this is the source of the difference between whole hippocampal analysis versus using dorsal hippocampal sections. It would thus be interesting in future studies to compare *Trem2* levels along the dorsal-ventral axis of the hippocampus from both mouse and man in the presence of the *Trem2*^{R47H} mutation when tissue becomes available in the future. Whatever the cause of the difference, the analysis gives insight into the role of TREM2. Moreover, the relatively small loss of expression in the Trem2^{R47H} mice is validated with the immunohistochemical signal in the present study.

The R47H mutation prevents the increase in *Trem2* expression in microglia that are touching plaques, but some microglia proliferation remains

Having verified in the regions tested that knockin of the *Trem2*^{R47H} mutation only slightly decreased *Trem2* expression in the absence of plaques, we went on to assess the effect of the mutation in relation to plaques. We thus compared microglial-enriched *Trem2* expression in NLFTrem2^{R47H} mice to the expression in NLF mice. The substantial increase in *Trem2* expression in microglia-touching plaques, observed in NLF mice, was almost completely absent in NLFTrem2^{R47H} mice, showing no significant difference between the plaque and peri-plaque regions (Figure 4A).

Interestingly, despite there being no significant increase in *Trem2* gene expression on the plaque in NLFTrem2^{R47H} mice, the microglial density is still increased by 20-fold on plaques compared with background. Similar to NLF, the microglial density was at background levels by 20 μm from the plaque. Thus increased *Trem2* expression is not necessary for microglial proliferation at the plaque.

Additionally, note that in the away from plaque AOIs in mice with plaques compared with the AOIs in mice without plaques, the NLF *App* genotype resulted in a strong trend to decreased Trem2 expression ($p = 0.052$), independent of *Trem2* genotype ($p = 0.16$) (Figure S5).

TREM2 protein levels largely confirm plaque dependence of *Trem2* expression

To assess if the remarkable fall off in *Trem2* expression away from plaques in NLF mice is reflected in a similar change in protein expression, we undertook an immunohistochemical analysis of TREM2 protein levels (Figures 4C, 4D, and S6). The analysis was restricted to TREM2 staining within IBA1-positive pixels. Fluorescence intensity was expressed per pixel to assess the expression within microglia, independent of density. Similar to the gene expression, there was an increase in TREM2 protein signal on the plaque in NLF mice, increasing 3-fold compared with levels away from plaques. The signal dropped rapidly to a plateau but, unlike gene expression, a small but significant increase was still detectable at 30 μm away from the plaque when compared with 50 μm, although this was not different from WT levels. Note, however, there is no change in microglial density in response to this more distal change in protein level.

In NLFTrem2^{R47H} mice, there was a significant increase in protein expression at the plaque and immediately adjacent to the plaque but to a significantly lower level than the NLF mice (Figures 4D and 4E). Notably, this small (1.6-fold) but significant increase in TREM2 protein did not apparently require a significant increase in gene expression in the NLFTrem2^{R47H} mice (Figure 4B), suggesting either increased translation or decreased clearance. Moreover, this related to a much greater (20-fold) increase in microglial density (Figure 4C).

The *Trem2*^{R47H} risk factor mutation prevents phagocytic phenotype and induces a higher density of small plaques

The question remains as to what the microglia clustered around the plaques are doing and what is the role of TREM2 in this activity. It has repeatedly been shown that an increase in *Trem2* expression results in increased phagocytosis[4,26,27] and that this is dependent on the *Trem2* genotype, with the R47H mutation decreasing the phagocytic activity.[28,29] In agreement with our previous report,[4] we observed the regional gene expression of *Cd68,* a marker of the phagocytic phenotype, and found that its expression mirrored that of *Trem2* and was similarly dependent on the *Trem2* genotype (Figure 5A). Hence in NLF mice, *Cd68* was only significantly upregulated in microglial-enriched AOIs that were on plaques and not in periplaque regions, and this increase was completely lost in the NLFTrem2^{R47H} mice. Immunohistochemical analysis was consistent with this result with CD68 protein levels in NLF mice being strongly upregulated in microglia on or immediately neighboring a plaque but returning to background level by 20 μm from the plaque. Furthermore, the upregulation of CD68 was dependent on the *Trem2* genotype (Figures 5B and 5C).

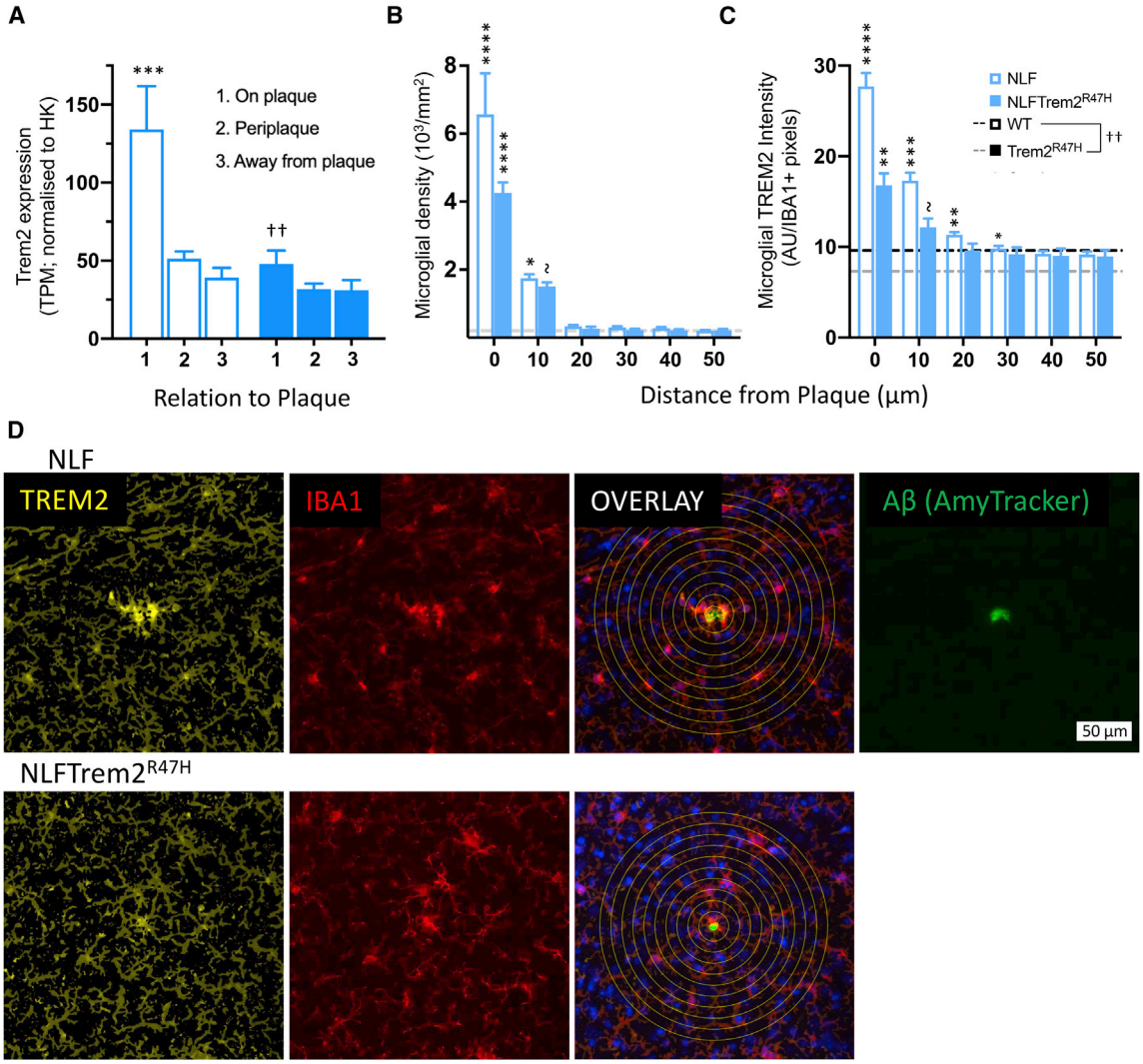

Figure 4. Increased microglia density at plaques is partially independent of *Trem2* genotype-dependent expression

(A) *Trem2* expression in NLF mice is significantly (2.6-fold) upregulated in microglial AOIs on plaques compared with periplaque AOIs. Periplaque AOIs are not significantly different from AOIs away from plaques or in WT mice. NLFTrem2^{R47H} mice show no difference on plaques compared with other regions in the same animals or compared with Trem2^{R47H} or WT mice. Two-way repeated measures ANOVA between NLF and NLFTrem2^{R47H} mice: main effects of relation to plaque ($p < 0.01$) and of genotype ($p < 0.01$) and near significant interaction ($p = 0.053$). *Post hoc* Sidak multiple comparison tests are shown on the graph: * within genotypes relative to NLF region 3 (away); † between genotype relative to NLF region1 (on plaque). NLF n = 6 mice; NLFTrem2^{R47H} n = 4 mice.

(B) Microglial density on plaques in NLFTrem2 mice is less than in NLF mice (60%, $p < 0.001$) but is increased >20-fold compared with WT or AOIs far from plaques, despite no significant change in *Trem2* expression. Two-way repeated measures ANOVA: main effect of distance from plaque ($p < 0.0001$); interaction between distance from plaque and genotype ($p = 0.014$). Sidak's multiple comparison test, * indicates a significant within genotype difference versus 50 μm from plaque. n = 6 mice per genotype.

(C) TREM2 protein levels reflect the distribution suggested by gene expression. Two-way repeated measures ANOVA: main effects of genotype, distance from plaque and interaction ($p < 0.0001$ in each case). *Post hoc* Sidak correction for multiple comparisons is shown on the graph. * compares within genotype versus 50 μm from plaque. Note that there is a significant difference in TREM2 signal of 20% between WT and Trem2^{R47H} mice ($p < 0.01$), * within genotype versus 50 μm from plaque; n = 11–12 mice for all genotypes, with approximately equal males and females. No significant effect of sex. All data are plotted as mean + SEM. ****$p < 0.0001$; ***$p < 0.001$; **/††$p < 0.01$; *$p < 0.05$ ~$p < 0.08$.

(D) Images of TREM2 staining comparing NLF and NLFTrem2^{R47H}. TREM2 (yellow); IBA1 microglia (red); Amytracker Aβ (green).

We then examined the plaque coverage and the number of plaques per area in the NLF and NLFTrem2^{R47H} mice. While the plaque coverage was not significantly different (Figure 5D), the number of plaques per area was greater in the NLFTrem2^{R47H} mice than in NLF mice (Figure 5E). We thus went on to analyze this apparent discrepancy by observing the number of plaques of different sizes. Most analysis around plaques, including the regional gene expression in the present study, concentrates on the large plaques, with cross-sectional area >~100 μm^2. These plaques dominate the plaque coverage

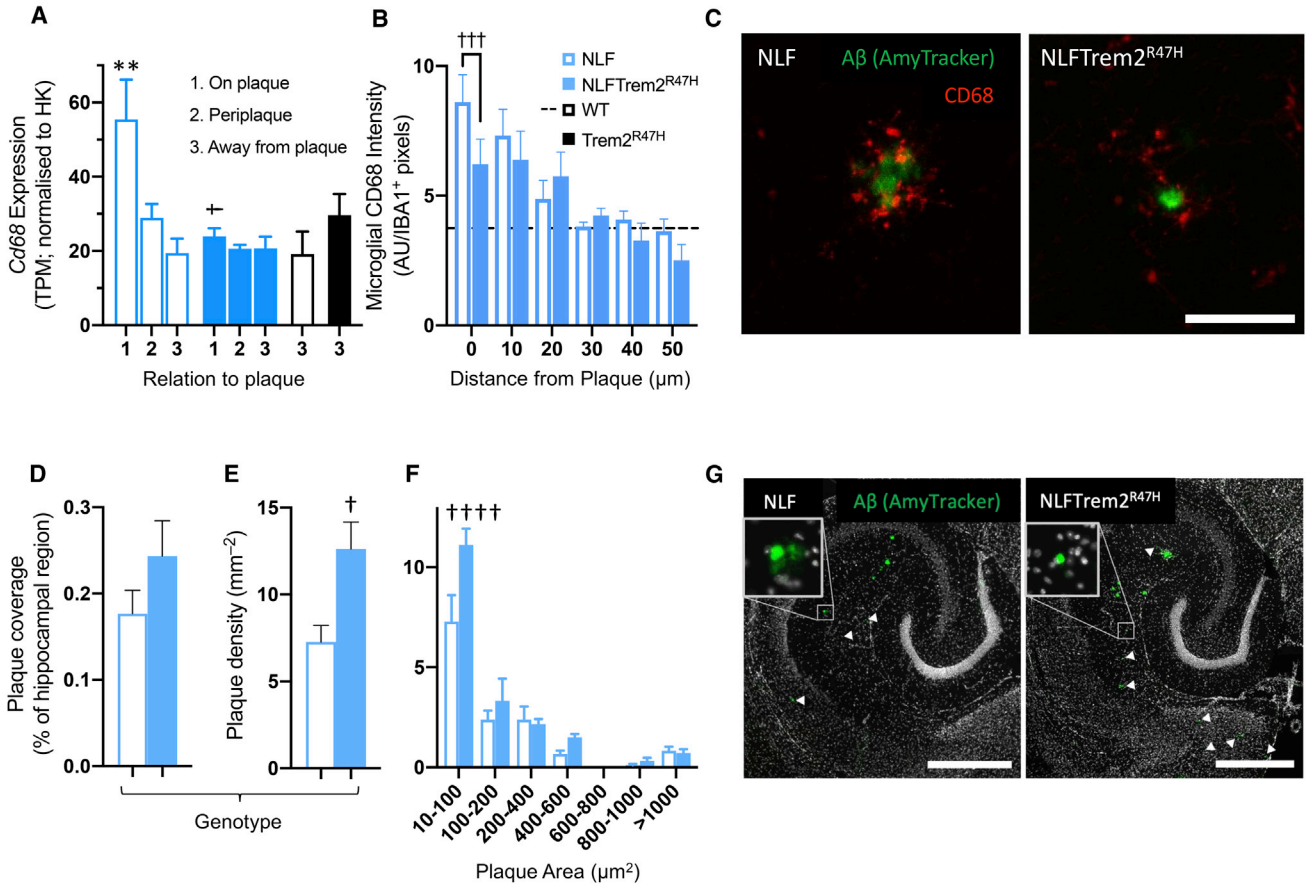

Figure 5. Microglial activation state and density of small plaques are affected by the *Trem2* genotype

(A) Expression of *Cd68* behaves similarly to *Trem2* expression, being significantly increased only in microglial AOIs touching plaques with the increased expression lost in the presence of the *Trem2*^{R47H} mutation. Sidak *post hoc* tests are indicated by * within genotype comparison versus group 3 (away). † indicates across genotype comparisons with respect to same AOI, $p < 0.05$. NLF: n = 6 mice; NLFTrem2^{R47H}, WT and Trem2^{R47H}, n = 4 mice per genotype.

(B and C) CD68 protein levels reflect the distribution suggested by gene expression. Two-way ANOVA: main effects of genotype ($p < 0.01$), distance from plaque ($p < 0.0001$), and interaction ($p < 0.001$). *Post hoc* Sidak correction for multiple comparisons across genotype is shown on the graph. NLF n = 5 mice; NLFTrem2^{R47H} n = 4 mice. Scale bar represents 50 µm.

(D and E) While plaque coverage did not show a significant difference between NLF and NLFTrem2^{R47H} mice (D), plaque density was higher in NLFTrem2^{R47H} versus the NLF mice (E).

(F) A plaque size-density frequency histogram revealed that the higher density of plaques was restricted to small plaques, Sidak *post hoc* tests across genotype, †$p < 0.05$, ††††$p < 0.0001$.

(G) Representative images of plaque size distribution in NLF and NLFTrem2^{R47H} mice. Scale bar represents 500 µm. Panels (D)–(F): n = 6 mice for both genotypes. Data are presented as mean + SEM in all panels. For all panels, ††††$p < 0.0001$; **/††$p < 0.01$; †$p < 0.05$.

of the brain regions studied. However, the majority of plaques, in terms of plaque number, are very small (<100 µm^2), and this remains true throughout age or stage of plaque development in both mice and humans.[13,30,31] When hippocampal plaque density was broken down by plaque size, the source of the difference was revealed to be entirely due to an increase of very small plaques in the NLFTrem2^{R47H} mice compared with the NLF mice (Figures 5F and 5G). This suggests that the microglia expressing high levels of *Trem2*^{WT} are not effective in phagocytosing large plaques. Either these microglia are instrumental in the removal of new small plaques or microglia with the *Trem2*^{R47H} mutation are causing the seeding of additional small plaques. However, in both scenarios, these small plaques are not developing into additional large plaques.

Only PIGs that depend on touching plaques for increased expression are dependent on *Trem2* genotype

The regional distributions of expression of PIGs were compared between NLF mice and NLFTrem2^{R47H} mice. Like *Trem2*, in six PIGs, (*C1qa*, *C1qc*, *Ctsz*, *Ctss*, *Grn*, *Plek*), the increased expression in microglia-touching plaques was prevented by the *Trem2*^{R47H} mutation (Figure 6). All of these genes fell into group 1, being only upregulated on plaques (Figure 3). This suggests that *Trem2*^{WT} is instrumental in the sharp upregulation of expression of these genes on the plaque. The distribution of expression changes of the other PIGs that were increased in expression in the plaque and/or periplaque areas was not significantly affected by the *Trem2*^{R47H} mutation (examples from each group in

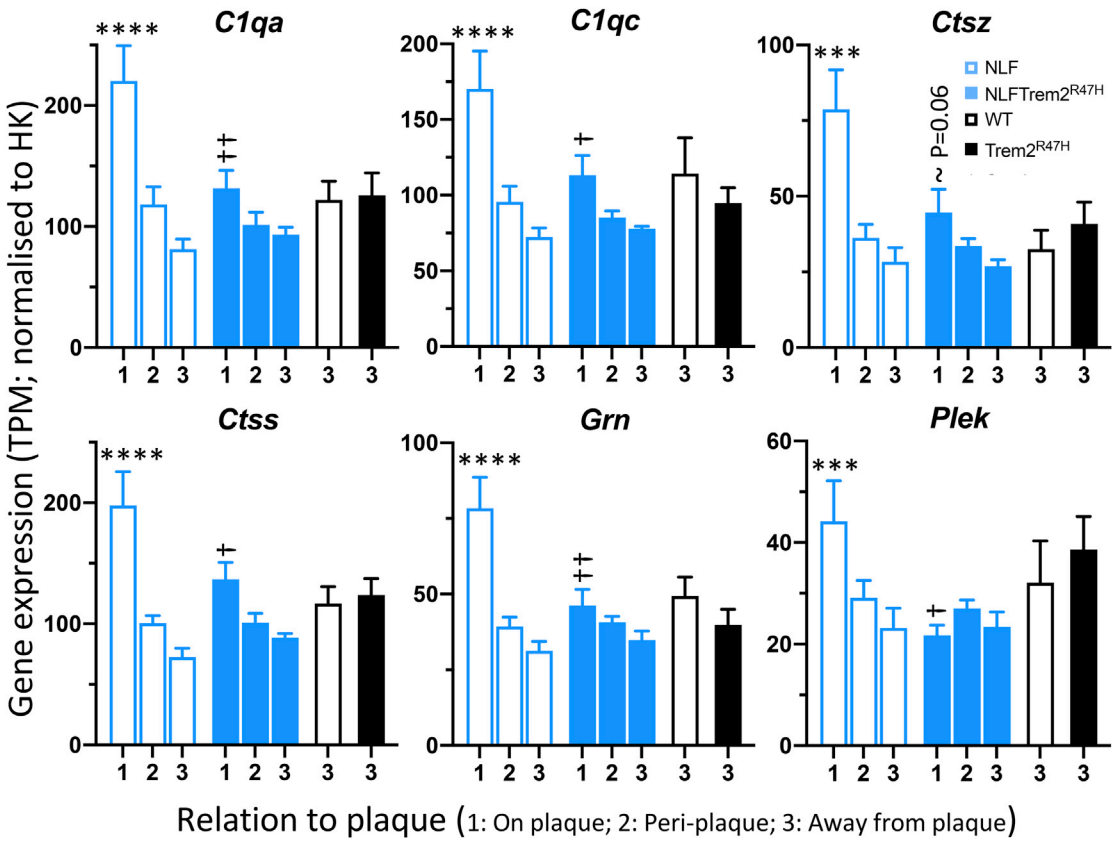

Figure 6. Upregulation of certain PIGs at plaques is dependent on *Trem2*^{R47H} genotype

Gene expression of six PIGs that showed a *Trem2*^{R47H}-dependent upregulation in plaque AOIs only. NLF: n = 6 mice; NLFTrem2^{R47H}, WT and Trem2^{R47H}, n = 4 mice per genotype. All data are plotted as mean + SEM. *Post hoc* Sidak multiple comparison tests are shown on the graphs. ****p < 0.0001; ***p < 0.001 within genotype compared with column 3 (away); **/††p < 0.01; †p < 0.05, between genotypes compared with NLF on-plaque. Also see Figure S7.

Figure S7). It is interesting to note that several of the genes that are upregulated on the plaque compared with the away region, independently of *Trem2*-genotype, show expression that is decreased in the area away from plaques compared with the levels in WT or Trem2^{R47H} mice. A striking example is the astrocytic GWAS risk gene, *Clu*.[32] This may reflect that the microglial AOI measurements of astrocytic genes are largely dependent on the degree of overlap of the remaining fine astrocytic processes (after the initial removal of the astrocyte AOIs). With astrogliosis probably showing an increase in spread of processes toward plaques, rather than proliferation or migration of cell bodies,[33,34] the fine processes stretching toward plaques may leave fewer processes in the away from plaque areas.

DISCUSSION

The observation that *Trem2* and related genes are strongly upregulated as plaques deposit in AD is well documented in studies of both mouse models[6,13] and human postmortem tissue.[3,35] Moreover, it has been repeatedly observed that the response of microglia around plaques is dependent on the *Trem2* genotype and is decreased with the *TREM2*^{R47H} risk factor mutation[36,37] or when *Trem2* is knocked out.[38] All the previous studies in Aβ mouse models have, however, relied either on aggressive transgenic models with overexpression of APP and the other problems of transgenic technology[39] or on NLGF knockin mice in which the plaques appear by 2 months and reach an almost maximal load rapidly during early life.[12,13,39] In the human sporadic condition, the development of plaques only starts in middle age, and it is in old age that the density of plaques and other factors combine to result in the well-known clinical outcomes. Rapid deposition of plaques in the brain of a young animal may have very different effects from the gradual deposition of plaques late in life, as occurs in the human condition.[40]

Although the NLF knockin mouse carries two familial AD mutations, it represents a model of disease in which the resulting rise in Aβ leads to a gradual rise in plaque load from 9 to 24 months of age.[13] This results in much more subtle changes in gene expression than the related NLGF mice or the many transgenic models that preceded it, and consequently, it has been more difficult to study with standard RNA-seq technology.

The introduction of spatial cell-type-enriched transcriptomics has allowed more detailed and higher resolution, allowing better detection of changes within individual brain sections, at different positions in relation to the plaques. Under these conditions, in analysis that pairs AOIs within the same sections, we found

that many, but not all, of the previously defined PIGs[11] were indeed increased in a plaque-related manner in NLF mice. The lack of apparent effect of vicinity of plaques in the present study of 17 of the 55 PIGs is most likely related to the different genotypes studied with Chen et al., having concentrated their study on NLGF mice that express plaques from 2 months of age and show a much stronger phenotype.[12,13] NLGF mice include an additional mutation within their Aβ sequence that results in a strong change in equilibrium of the Aβ toward deposition. Hence it may be, in even older NLF mice with heavier plaque loads, that these genes would be upregulated, or otherwise that these 17 genes are upregulated because of the deposition of a different Aβ structure at a much younger age and would not translate to the human condition. Alternatively, the difference may be related to the different methods used, with the present study relating gene expression to distance from plaque in cell-type-enriched AOIs, while the Chen study only used plaque density without focusing on cell type. Consequently, depending on the cell types in which genes are expressed, this could lead to different results between the two studies. Indeed, the 30% of the PIGs that did not come out in the present analysis as being differentially expressed in relation to distance from plaque had been previously identified as genes highly expressed in other cell types such as oligodendrocytes, epithelial cells, or astrocytes.[14,15]

Strikingly, in the present study, a subset of the genes, including *Trem2,* were only increased in the microglia AOIs that were on plaques and not in the immediately adjacent regions. Moreover, in the case of seven of these genes, this tight regional increase in expression was not only dependent on the microglia touching the plaques but was strongly dependent on the *Trem2* genotype. Although we cannot exclude the possibility that a subset of the microglia in the periplaque region also upregulates these genes, this is clearly not the dominant response. This dependence on plaque contact in a Trem2 genotype-dependent manner confirms the very tight interaction between plaques and microglial genes but refines the module to a much smaller and more clearly related group. The module includes the *C1q* complement factors that have consistently been associated with *Trem2* expression in AD mouse models.[6] However, the other genes are associated with the phagosome (*Plek*)[41] or lysosomal function (*Ctsz*, *Ctss*, and *Grn*).[42–45] All of these genes are linked with the dependence on the *Trem2* genotype suggesting that $Trem2^{WT}$ is the essential controller. The observation that they only upregulate in microglia-touching plaques suggests that the TREM2 ligand that sets this chain in motion is either lipophilic or otherwise restricted to the plaque, rather than a signal diffusing away from the plaque. A possible candidate would be a phospholipid, such as phosphotidylserine that has been suggested to be an "eat me" signal on damaged synapses.[46,47] This is consistent with a role for microglia in removing Aβ-induced dystrophic synapses to limit the spread of damage along axons or dendrites.[48] The cascade then proceeds via C1Q and the complement pathway, leading to phagocytosis involving pleckstrin and subsequent lysosomal removal of waste involving the cathepsins, NPC2, and progranulin. In principle, this involves activation of proteins and does not need to involve gene expression if sufficient protein is already expressed by the microglia. However, the increased expression of all these genes suggests that these may be rate-limiting steps in the process. This is further underlined by the fact that some increase in protein and considerable microglial proliferation occur in $NLFTrem2^{R47H}$ knockin mice, despite a lack of differential expression of *Trem2* at the plaque, with the modest increase in translation of protein being apparently sufficient.

The link between this subset of PIGs leading to the phagocytic phenotype of microglia is further supported by the expression of the phagocytic marker CD68[49] that shows the same behavior, being only upregulated on plaques and dependent on the $Trem2^{WT}$ genotype. Although, it should be noted that *Cd68* is not included in the genes reported to be plaque induced by Chen et al.

An alternative hypothesis for the role of this phagocytic pathway, not mutually exclusive from the above, suggests that the role of plaque-related microglial phagocytosis relates to removal of Aβ.[50] In this context, several studies have investigated the effect of removing microglia using inhibitors of the CSF1 receptor.[13,51–53] Together, these studies suggest that microglia may have a role in seeding new plaques, but that the overall plaque load, once established, is little affected by the removal of microglia.[54] In the present study, we found a notable effect of the *Trem2* genotype in that $NLFTrem2^{R47H}$ mice showed a selective increase in the number of very small plaques compared with NLF mice, while larger plaques were unaffected. This is largely consistent with the findings above. It seems that the activation of microglia expressing $Trem2^{WT}$ may be involved in the removal of very small plaques, but once the plaques grow past about 100 μm^2, they are no longer effective in their removal. An alternative explanation could be that the $Trem2^{R47H}$ mutation results in constant seeding of plaques either *de novo*[55] or by small plaques breaking off from the larger plaques. However, it seems that these extra plaques are not destined to grow. It should also be noted that it seems unlikely that Aβ is the ligand triggering the response as soluble Aβ would be expected to be present at a distance from the plaque in NLF mice, whereas the present data suggest that the cascade is only triggered once the microglia come physically in contact with plaque.

Limitations of the study

The transcriptomic analysis in this study was carried out in 8-μm-thick sections, and the RNA probe-associated DNA oligo tags were cleaved by laser application that would penetrate the whole depth of the tissue. Hence, where synapses or other cell types were above or below the microglial AOI, transcripts from these other cell types would also be detected. Moreover, the area sampled was dependent on the limitations of the visualization and filter settings used. While this was consistent throughout and so would affect all areas equally, it means that the results are enriched for microglial transcripts but neither entirely specific for this cell type nor guaranteed to capture all microglia or the full area of every microglial cell visualized. Moreover, this also applies to the visualization of plaques, so that the detection of the plaque edge was dependent on filter settings used. Therefore, although we can be confident that on plaque, microglia are indeed touching plaques, some microglia touching the edge of the plaque could be classified as periplaque microglia. This would however largely lead to a

decrease in the primary differences reported in this study (in genes only increased on plaques). Other limitations come from the limitations of the mouse model. Like all models, the NLF mouse model has limitations. Apart from the general differences of mouse and man, this is a model of early plaque progression and does not lead to the development of neurofibrillary tangles and substantial neurodegeneration that would be the equivalent of the diagnosed stages of AD. Moreover, the Trem2^{R47H} KI mouse model has been reported to show a decrease in *Trem2* expression. Hence the NLFTrem2 mice are a model both of somewhat decreased TREM2 level as well as loss of function due to the mutation.

Conclusions

Use of spatial cell-enriched transcriptomics has allowed analysis of plaque-related gene expression in a mouse model that mimics the slow and age-related deposition in plaques that is seen in AD. The findings in the present study confirm the basic principles of much that has been shown in more aggressive models in which plaque load increases rapidly over early life.[6,11] However, it refines the effects to a smaller group of genes closely related to *Trem2* expression and dependent on the *Trem2* genotype. The comparison of the dependence of the expression of these genes on microglia-touching plaques and the differential dependence on *Trem2* genotype of microglial density strongly suggests that the increase of microglial density is, at most, marginally dependent on *Trem2* genotype. Moreover, the increase in expression of this group of genes appears to depend on a ligand that does not diffuse far from plaques.

STAR★METHODS

Detailed methods are provided in the online version of this paper and include the following:

- KEY RESOURCES TABLE
- RESOURCE AVAILABILITY
  - Lead contact
  - Materials availability
  - Data and code availability
- EXPERIMENTAL MODEL AND SUBJECT DETAILS
  - Mice
- METHOD DETAILS
  - Genotyping
  - Tissue extraction
  - Sectioning
  - Nanostring GeoMx digital spatial profiler
  - Region of interest (ROI) selection
  - Area of interest (AOI) selection
  - Library preparation and readout
  - Analysis
  - Histology
  - Imaging for immunohistochemistry
  - Protein intensity analysis
  - Microglial density analysis
- QUANTIFICATION AND STATISTICAL ANALYSIS
  - Statistical analysis
- ADDITIONAL RESOURCES

SUPPLEMENTAL INFORMATION

Supplemental information can be found online at https://doi.org/10.1016/j.celrep.2022.111686.

ACKNOWLEDGMENTS

This work was largely funded by a grant from Alzheimer's Research UK (F.A.E. and D.M.C.) and The Cure Alzheimer's Fund (F.A.E. and J.H.). J.H. is supported by the Dana Foundation. His work was partly funded by the UK DRI, which receives its funding from the DRI Ltd, funded by the UK Medical Research Council. J.I.W. is funded by the Swedish Alzheimer's Foundation, and K.S.V. was funded by a studentship from the UK Medical Research Council.

AUTHOR CONTRIBUTIONS

Conceptualization: F.A.E. and J.I.W. Methodology: F.A.E., D.M.C., J.I.W., A.V., and R.J. Investigation: J.I.W., E.W., R.J., K.S.V., S.D., A.B., S.-L.J.P., F.L., and K.S. Visualization: F.A.E., J.I.W., and D.M.C. Supervision: D.M.C., F.A.E., and T.T. Writing – original draft: F.A.E. and J.I.W. Writing – review & editing: J.I.W., J. Hardy, D.M.C., and F.A.E. (all authors). Funding: F.A.E., D.M.C., J. Hardy, and J. Hanrieder.

DECLARATION OF INTERESTS

A.V. and S.-L.J.P. were employed by Nanostring Technologies.

Received: February 22, 2022
Revised: August 30, 2022
Accepted: October 27, 2022
Published: November 22, 2022

REFERENCES

1. Guerreiro, R., Wojtas, A., Bras, J., Carrasquillo, M., Rogaeva, E., Majounie, E., Cruchaga, C., Sassi, C., Kauwe, J.S., Younkin, S., et al. (2013). TREM2 variants in Alzheimer's disease. N. Engl. J. Med. *368*, 117–127. https://doi.org/10.1056/NEJMoa1211851.
2. Jonsson, T., Stefansson, H., Steinberg, S., Jonsdottir, I., Jonsson, P.V., Snaedal, J., Bjornsson, S., Huttenlocher, J., Levey, A.I., Lah, J.J., et al. (2013). Variant of TREM2 associated with the risk of Alzheimer's disease. N. Engl. J. Med. *368*, 107–116. https://doi.org/10.1056/NEJMoa1211103.
3. Gratuze, M., Leyns, C.E.G., and Holtzman, D.M. (2018). New insights into the role of TREM2 in Alzheimer's disease. Mol. Neurodegener. *13*, 66. https://doi.org/10.1186/s13024-018-0298-9.
4. Liu, W., Taso, O., Wang, R., Bayram, S., Graham, A.C., Garcia-Reitboeck, P., Mallach, A., Andrews, W.D., Piers, T.M., Botia, J.A., et al. (2020). Trem2 promotes anti-inflammatory responses in microglia and is suppressed under pro-inflammatory conditions. Hum. Mol. Genet. *29*, 3224–3248. https://doi.org/10.1093/hmg/ddaa209.
5. Kulkarni, B., Kumar, D., Cruz-Martins, N., and Sellamuthu, S. (2021). Role of TREM2 in alzheimer's disease: a long road ahead. Mol. Neurobiol. *58*, 5239–5252. https://doi.org/10.1007/s12035-021-02477-9.
6. Matarin, M., Salih, D.A., Yasvoina, M., Cummings, D.M., Guelfi, S., Liu, W., Nahaboo Solim, M.A., Moens, T.G., Paublete, R.M., Ali, S.S., et al. (2015). A genome-wide gene-expression analysis and database in transgenic mice during development of amyloid or tau pathology. Cell Rep. *10*, 633–644. https://doi.org/10.1016/j.celrep.2014.12.041.
7. Salih, D.A., Bayram, S., Guelfi, S., Reynolds, R.H., Shoai, M., Ryten, M., Brenton, J.W., Zhang, D., Matarin, M., Botia, J.A., et al. (2019). Genetic variability in response to amyloid beta deposition influences Alzheimer's disease risk. Brain Commun. *1*, fcz022. https://doi.org/10.1093/braincomms/fcz022.

8. Deczkowska, A., Keren-Shaul, H., Weiner, A., Colonna, M., Schwartz, M., and Amit, I. (2018). Disease-associated microglia: a universal immune sensor of neurodegeneration. Cell *173*, 1073–1081. https://doi.org/10.1016/j.cell.2018.05.003.

9. Keren-Shaul, H., Spinrad, A., Weiner, A., Matcovitch-Natan, O., Dvir-Szternfeld, R., Ulland, T.K., David, E., Baruch, K., Lara-Astaiso, D., Toth, B., et al. (2017). A unique microglia type Associated with restricting development of alzheimer's disease. Cell *169*, 1276–1290.e17. https://doi.org/10.1016/j.cell.2017.05.018.

10. Lee, S.H., Meilandt, W.J., Xie, L., Gandham, V.D., Ngu, H., Barck, K.H., Rezzonico, M.G., Imperio, J., Lalehzadeh, G., Huntley, M.A., et al. (2021). Trem2 restrains the enhancement of tau accumulation and neurodegeneration by beta-amyloid pathology. Neuron *109*, 1283–1301.e6. https://doi.org/10.1016/j.neuron.2021.02.010.

11. Chen, W.T., Lu, A., Craessaerts, K., Pavie, B., Sala Frigerio, C., Corthout, N., Qian, X., Lalakova, J., Kuhnemund, M., Voytyuk, I., et al. (2020). Spatial transcriptomics and in situ sequencing to study alzheimer's disease. Cell *182*, 976–991.e19. https://doi.org/10.1016/j.cell.2020.06.038.

12. Saito, T., Matsuba, Y., Mihira, N., Takano, J., Nilsson, P., Itohara, S., Iwata, N., and Saido, T.C. (2014). Single App knock-in mouse models of Alzheimer's disease. Nat. Neurosci. *17*, 661–663. https://doi.org/10.1038/nn.3697.

13. Benitez, D.P., Jiang, S., Wood, J., Wang, R., Hall, C.M., Peerboom, C., Wong, N., Stringer, K.M., Vitanova, K.S., Smith, V.C., et al. (2021). Knock-in models related to Alzheimer's disease: synaptic transmission, plaques and the role of microglia. Mol. Neurodegener. *16*, 47. https://doi.org/10.1186/s13024-021-00457-0.

14. Ximerakis, M., Lipnick, S.L., Innes, B.T., Simmons, S.K., Adiconis, X., Dionne, D., Mayweather, B.A., Nguyen, L., Niziolek, Z., Ozek, C., et al. (2019). Single-cell transcriptomic profiling of the aging mouse brain. Nat. Neurosci. *22*, 1696–1708. https://doi.org/10.1038/s41593-019-0491-3.

15. Zhang, Y., Chen, K., Sloan, S.A., Bennett, M.L., Scholze, A.R., O'Keeffe, S., Phatnani, H.P., Guarnieri, P., Caneda, C., Ruderisch, N., et al. (2014). An RNA-sequencing transcriptome and splicing database of glia, neurons, and vascular cells of the cerebral cortex. J. Neurosci. *34*, 11929–11947. https://doi.org/10.1523/JNEUROSCI.1860-14.2014.

16. Grubman, A., Choo, X.Y., Chew, G., Ouyang, J.F., Sun, G., Croft, N.P., Rossello, F.J., Simmons, R., Buckberry, S., Landin, D.V., et al. (2021). Transcriptional signature in microglia associated with Abeta plaque phagocytosis. Nat. Commun. *12*, 3015. https://doi.org/10.1038/s41467-021-23111-1.

17. Robinson, M.D., and Oshlack, A. (2010). A scaling normalization method for differential expression analysis of RNA-seq data. Genome Biol. *11*, R25. https://doi.org/10.1186/gb-2010-11-3-r25.

18. Itagaki, S., McGeer, P.L., Akiyama, H., Zhu, S., and Selkoe, D. (1989). Relationship of microglia and astrocytes to amyloid deposits of Alzheimer disease. J. Neuroimmunol. *24*, 173–182. https://doi.org/10.1016/0165-5728(89)90115-x.

19. Medawar, E., Benway, T.A., Liu, W., Hanan, T.A., Haslehurst, P., James, O.T., Yap, K., Muessig, L., Moroni, F., Nahaboo Solim, M.A., et al. (2019). Effects of rising amyloidbeta levels on hippocampal synaptic transmission, microglial response and cognition in APPSwe/PSEN1M146V transgenic mice. EBioMedicine *39*, 422–435. https://doi.org/10.1016/j.ebiom.2018.12.006.

20. Hammarstrom, P., Simon, R., Nystrom, S., Konradsson, P., Aslund, A., and Nilsson, K.P. (2010). A fluorescent pentameric thiophene derivative detects in vitro-formed prefibrillar protein aggregates. Biochemistry *49*, 6838–6845. https://doi.org/10.1021/bi100922r.

21. Klingstedt, T., Aslund, A., Simon, R.A., Johansson, L.B., Mason, J.J., Nystrom, S., Hammarstrom, P., and Nilsson, K.P. (2011). Synthesis of a library of oligothiophenes and their utilization as fluorescent ligands for spectral assignment of protein aggregates. Org. Biomol. Chem. *9*, 8356–8370. https://doi.org/10.1039/c1ob05637a.

22. Klingstedt, T., Blechschmidt, C., Nogalska, A., Prokop, S., Haggqvist, B., Danielsson, O., Engel, W.K., Askanas, V., Heppner, F.L., and Nilsson, K.P. (2013). Luminescent conjugated oligothiophenes for sensitive fluorescent assignment of protein inclusion bodies. Chembiochem *14*, 607–616. https://doi.org/10.1002/cbic.201200731.

23. Cheng-Hathaway, P.J., Reed-Geaghan, E.G., Jay, T.R., Casali, B.T., Bemiller, S.M., Puntambekar, S.S., von Saucken, V.E., Williams, R.Y., Karlo, J.C., Moutinho, M., et al. (2018). The Trem2 R47H variant confers loss-of-function-like phenotypes in Alzheimer's disease. Mol. Neurodegener. *13*, 29. https://doi.org/10.1186/s13024-018-0262-8.

24. Xiang, X., Piers, T.M., Wefers, B., Zhu, K., Mallach, A., Brunner, B., Kleinberger, G., Song, W., Colonna, M., Herms, J., et al. (2018). The Trem2 R47H Alzheimer's risk variant impairs splicing and reduces Trem2 mRNA and protein in mice but not in humans. Mol. Neurodegener. *13*, 49. https://doi.org/10.1186/s13024-018-0280-6.

25. Vogel, J.W., La Joie, R., Grothe, M.J., Diaz-Papkovich, A., Doyle, A., Vachon-Presseau, E., Lepage, C., Vos de Wael, R., Thomas, R.A., Iturria-Medina, Y., et al. (2020). A molecular gradient along the longitudinal axis of the human hippocampus informs large-scale behavioral systems. Nat. Commun. *11*, 960. https://doi.org/10.1038/s41467-020-14518-3.

26. Takahashi, K., Rochford, C.D., and Neumann, H. (2005). Clearance of apoptotic neurons without inflammation by microglial triggering receptor expressed on myeloid cells-2. J. Exp. Med. *201*, 647–657. https://doi.org/10.1084/jem.20041611.

27. Jiang, T., Wan, Y., Zhang, Y.D., Zhou, J.S., Gao, Q., Zhu, X.C., Shi, J.Q., Lu, H., Tan, L., and Yu, J.T. (2017). TREM2 overexpression has No improvement on neuropathology and cognitive impairment in aging APPswe/PS1dE9 mice. Mol. Neurobiol. *54*, 855–865. https://doi.org/10.1007/s12035-016-9704-x.

28. Yin, J., Liu, X., He, Q., Zhou, L., Yuan, Z., and Zhao, S. (2016). Vps35-dependent recycling of Trem2 regulates microglial function. Traffic *17*, 1286–1296. https://doi.org/10.1111/tra.12451.

29. Kleinberger, G., Yamanishi, Y., Suarez-Calvet, M., Czirr, E., Lohmann, E., Cuyvers, E., Struyfs, H., Pettkus, N., Wenninger-Weinzierl, A., Mazaheri, F., et al. (2014). TREM2 mutations implicated in neurodegeneration impair cell surface transport and phagocytosis. Sci. Transl. Med. *6*, 243ra286. https://doi.org/10.1126/scitranslmed.3009093.

30. Morris, J.C., Storandt, M., McKeel, D.W., Jr., Rubin, E.H., Price, J.L., Grant, E.A., and Berg, L. (1996). Cerebral amyloid deposition and diffuse plaques in "normal" aging: evidence for presymptomatic and very mild Alzheimer's disease. Neurology *46*, 707–719. https://doi.org/10.1212/wnl.46.3.707.

31. Murray, M.E., and Dickson, D.W. (2014). Is pathological aging a successful resistance against amyloid-beta or preclinical Alzheimer's disease? Alzheimer's Res. Ther. *6*, 24. https://doi.org/10.1186/alzrt254.

32. Schwartzentruber, J., Cooper, S., Liu, J.Z., Barrio-Hernandez, I., Bello, E., Kumasaka, N., Young, A.M.H., Franklin, R.J.M., Johnson, T., Estrada, K., et al. (2021). Genome-wide meta-analysis, fine-mapping and integrative prioritization implicate new Alzheimer's disease risk genes. Nat. Genet. *53*, 392–402. https://doi.org/10.1038/s41588-020-00776-w.

33. Damisah, E.C., Hill, R.A., Rai, A., Chen, F., Rothlin, C.V., Ghosh, S., and Grutzendler, J. (2020). Astrocytes and microglia play orchestrated roles and respect phagocytic territories during neuronal corpse removal in vivo. Sci. Adv. *6*, eaba3239. https://doi.org/10.1126/sciadv.aba3239.

34. Bardehle, S., Kruger, M., Buggenthin, F., Schwausch, J., Ninkovic, J., Clevers, H., Snippert, H.J., Theis, F.J., Meyer-Luehmann, M., Bechmann, I., et al. (2013). Live imaging of astrocyte responses to acute injury reveals selective juxtavascular proliferation. Nat. Neurosci. *16*, 580–586. https://doi.org/10.1038/nn.3371.

35. Jay, T.R., Miller, C.M., Cheng, P.J., Graham, L.C., Bemiller, S., Broihier, M.L., Xu, G., Margevicius, D., Karlo, J.C., Sousa, G.L., et al. (2015). TREM2 deficiency eliminates TREM2+ inflammatory macrophages and ameliorates pathology in Alzheimer's disease mouse models. J. Exp. Med. *212*, 287–295. https://doi.org/10.1084/jem.20142322.

36. Korvatska, O., Leverenz, J.B., Jayadev, S., McMillan, P., Kurtz, I., Guo, X., Rumbaugh, M., Matsushita, M., Girirajan, S., Dorschner, M.O., et al. (2015). R47H variant of TREM2 associated with alzheimer disease in a large late-onset family: clinical, genetic, and neuropathological study. JAMA Neurol. *72*, 920–927. https://doi.org/10.1001/jamaneurol.2015.0979.

37. Song, W.M., Joshita, S., Zhou, Y., Ulland, T.K., Gilfillan, S., and Colonna, M. (2018). Humanized TREM2 mice reveal microglia-intrinsic and -extrinsic effects of R47H polymorphism. J. Exp. Med. *215*, 745–760. https://doi.org/10.1084/jem.20171529.

38. McQuade, A., Kang, Y.J., Hasselmann, J., Jairaman, A., Sotelo, A., Coburn, M., Shabestari, S.K., Chadarevian, J.P., Fote, G., Tu, C.H., et al. (2020). Gene expression and functional deficits underlie TREM2-knockout microglia responses in human models of Alzheimer's disease. Nat. Commun. *11*, 5370. https://doi.org/10.1038/s41467-020-19227-5.

39. Sasaguri, H., Nilsson, P., Hashimoto, S., Nagata, K., Saito, T., De Strooper, B., Hardy, J., Vassar, R., Winblad, B., and Saido, T.C. (2017). APP mouse models for Alzheimer's disease preclinical studies. EMBO J. *36*, 2473–2487. https://doi.org/10.15252/embj.201797397.

40. Stam, F.C., Wigboldus, J.M., and Smeulders, A.W. (1986). Age incidence of senile brain amyloidosis. Pathol. Res. Pract. *181*, 558–562. https://doi.org/10.1016/S0344-0338(86)80149-2.

41. Brumell, J.H., Howard, J.C., Craig, K., Grinstein, S., Schreiber, A.D., and Tyers, M. (1999). Expression of the protein kinase C substrate pleckstrin in macrophages: association with phagosomal membranes. J. Immunol. *163*, 3388–3395.

42. Lee, J.Y., Marian, O.C., and Don, A.S. (2021). Defective lysosomal lipid catabolism as a common pathogenic mechanism for dementia. NeuroMolecular Med. *23*, 1–24. https://doi.org/10.1007/s12017-021-08644-4.

43. Infante, R.E., Wang, M.L., Radhakrishnan, A., Kwon, H.J., Brown, M.S., and Goldstein, J.L. (2008). NPC2 facilitates bidirectional transfer of cholesterol between NPC1 and lipid bilayers, a step in cholesterol egress from lysosomes. Proc. Natl. Acad. Sci. *105*, 15287–15292. https://doi.org/10.1073/pnas.0807328105.

44. Tjondrokoesoemo, A., Schips, T.G., Sargent, M.A., Vanhoutte, D., Kanisicak, O., Prasad, V., Lin, S.C., Maillet, M., and Molkentin, J.D. (2016). Cathepsin S contributes to the pathogenesis of muscular dystrophy in mice. J. Biol. Chem. *291*, 9920–9928. https://doi.org/10.1074/jbc.M116.719054.

45. Paushter, D.H., Du, H., Feng, T., and Hu, F. (2018). The lysosomal function of progranulin, a guardian against neurodegeneration. Acta Neuropathol. *136*, 1–17. https://doi.org/10.1007/s00401-018-1861-8.

46. Scott-Hewitt, N., Perrucci, F., Morini, R., Erreni, M., Mahoney, M., Witkowska, A., Carey, A., Faggiani, E., Schuetz, L.T., Mason, S., et al. (2020). Local externalization of phosphatidylserine mediates developmental synaptic pruning by microglia. EMBO J. *39*, e105380. https://doi.org/10.15252/embj.2020105380.

47. Kober, D.L., and Brett, T.J. (2017). TREM2-Ligand interactions in health and disease. J. Mol. Biol. *429*, 1607–1629. https://doi.org/10.1016/j.jmb.2017.04.004.

48. Edwards, F.A. (2019). A unifying hypothesis for alzheimer's disease: from plaques to neurodegeneration. Trends Neurosci. *42*, 310–322. https://doi.org/10.1016/j.tins.2019.03.003.

49. Zotova, E., Holmes, C., Johnston, D., Neal, J.W., Nicoll, J.A., and Boche, D. (2011). Microglial alterations in human Alzheimer's disease following Abeta42 immunization. Neuropathol. Appl. Neurobiol. *37*, 513–524. https://doi.org/10.1111/j.1365-2990.2010.01156.x.

50. Yu, Y., and Ye, R.D. (2015). Microglial Abeta receptors in Alzheimer's disease. Cell. Mol. Neurobiol. *35*, 71–83. https://doi.org/10.1007/s10571-014-0101-6.

51. Dagher, N.N., Najafi, A.R., Kayala, K.M., Elmore, M.R., White, T.E., Medeiros, R., West, B.L., and Green, K.N. (2015). Colony-stimulating factor 1 receptor inhibition prevents microglial plaque association and improves cognition in 3xTg-AD mice. J. Neuroinflammation *12*, 139. https://doi.org/10.1186/s12974-015-0366-9.

52. Spangenberg, E., Severson, P.L., Hohsfield, L.A., Crapser, J., Zhang, J., Burton, E.A., Zhang, Y., Spevak, W., Lin, J., Phan, N.Y., et al. (2019). Sustained microglial depletion with CSF1R inhibitor impairs parenchymal plaque development in an Alzheimer's disease model. Nat. Commun. *10*, 3758. https://doi.org/10.1038/s41467-019-11674-z.

53. Spangenberg, E.E., Lee, R.J., Najafi, A.R., Rice, R.A., Elmore, M.R., Blurton-Jones, M., West, B.L., and Green, K.N. (2016). Eliminating microglia in Alzheimer's mice prevents neuronal loss without modulating amyloid-β pathology. Brain *139*, 1265–1281. https://doi.org/10.1093/brain/aww016.

54. Zhao, R., Hu, W., Tsai, J., Li, W., and Gan, W.B. (2017). Microglia limit the expansion of beta-amyloid plaques in a mouse model of Alzheimer's disease. Mol. Neurodegener. *12*, 47. https://doi.org/10.1186/s13024-017-0188-6.

55. Friedrich, R.P., Tepper, K., Ronicke, R., Soom, M., Westermann, M., Reymann, K., Kaether, C., and Fandrich, M. (2010). Mechanism of amyloid plaque formation suggests an intracellular basis of Abeta pathogenicity. Proc. Natl. Acad. Sci. USA *107*, 1942–1947. https://doi.org/10.1073/pnas.0904532106.

56. Schindelin, J., Arganda-Carreras, I., Frise, E., Kaynig, V., Longair, M., Pietzsch, T., Preibisch, S., Rueden, C., Saalfeld, S., Schmid, B., et al. (2012). Fiji: an open-source platform for biological-image analysis. Nat. Methods *9*, 676–682. https://doi.org/10.1038/nmeth.2019.

STAR★METHODS

KEY RESOURCES TABLE

REAGENT or RESOURCE	SOURCE	IDENTIFIER
Antibodies		
Mouse anti-Aβ40/42, Alexa Fluor 594	Nanostring Technologies	Cat#121301306
Mouse anti-GFAP, Alexa Fluor 488	Invitrogen	Cat#53-9892-82 RRID:AB_10598515
Rabbit anti-TMEM119	SynapticSystems	Cat#400002 RRID:AB_2721104
SYTO 13	Invitrogen	Cat#S7575
Rabbit anti-IBA1	FujiFilm Wako Chemicals	Cat#019-19741 RRID:AB_839504
Sheep anti-TREM2	R&D Systems	Cat#AF1729 RRID:AB_354956
Rat anti-CD68	Biorad	Cat#MCA1957 RRID:AB_322219
Goat anti-rabbit Alexa Fluor 647	Thermo Fisher Scientific	Cat#A11037 RRID:AB_2534095
Donkey anti-rabbit Alexa Fluor 594	Invitrogen	Cat#A32754 RRID:AB_2762827
Donkey anti-sheep Alexa Fluor 647	Abcam	Cat#AB150179 RRID:AB_2884038
Goat anti-rat Alexa Fluor 594	Abcam	Cat#AB150160 RRID:AB_2756445
Chemicals, peptides, and recombinant proteins		
Amytracker520	Ebba Biotech	Cat#A520-50
DAPI (4′,6-diamidino-2-phenylindole)	Thermo Fisher Scientific	Cat#D1306
Critical commercial assays		
Nanostring GeoMx Digital Spatial Profiler (DSP)	Nanostring	https://nanostring.com/products/geomx-digital-spatial-profiler/geomx-dsp-overview
Deposited data		
Mouseac gene database	This manuscript	https://edwardslab.shinyapps.io/MouseacST/
Experimental models: Organisms/strains		
mouse: C57BL/6: C57BL/6NCrl	Charles River	Strain#027
mouse: $APP^{NL\text{-}F/NL\text{-}F}$: C57BL/6-$App^{tm2.1Tcs}$	Saito et al.[12]	Available from the Saido lab
mouse: $Trem2^{R47H/R47H}$: C57BL/6J-$Trem2^{em1Adiuj}$/J	Jackson Laboratory	Strain#027918
mouse: $APP^{NL\text{-}F/NL\text{-}F}xTrem2^{R47H/R47H}$	This manuscript	Available from Edwards lab if permission obtained from Riken and Jackson Laboratory
Software and algorithms		
Plaque Concentric Circle Spatial Analysis	Developed In Edwards Lab	https://doi.org/10.5281/zenodo.5847431
Fiji/ImageJ	Schindelin et al.[56]	https://imagej.nih.gov/ij/
Graphpad Prism v9.2	Graphpad	https://www.graphpad.com/scientific-software/prism/

RESOURCE AVAILABILITY

Lead contact

Further information and requests for resources and reagents should be directed to and will be fulfilled by the lead contact, Frances Edwards (f.a.edwards@ucl.ac.uk).

Materials availability

The *App*$^{NL\text{-}F/NL\text{-}F}$x*Trem2*$^{R47H/R47H}$ mouse line generated in this study Is restricted due to breeder MTAs from The Jackson Laboratory (Bar Harbor, ME, USA) and RIKEN Centre (Yokohama, Japan).

Data and code availability

All data reported in this paper will be shared by the lead contact upon request. This paper does not report original code. Any additional information required to reanalyze the data reported in this paper is available from the lead contact upon request.

EXPERIMENTAL MODEL AND SUBJECT DETAILS

Mice

Male and female 18-month-old *App*$^{NL-F/NL-F}$ knock-in mice (NLF), *App*$^{NL-F/NL-F}$ knock-in mice harbouring the *Trem2*$^{R47H/R47H}$ mutation (NLFTrem2^{R47H}) and age-matched C57BL/6J (WT) and *Trem2*$^{R47H/R47H}$ (Trem2^{R47H}) control mice were used throughout the study. No statistically significant sex differences were observed. All mice were bred in the UCL Biological Services Unit. Original breeders for the NLF mice were obtained from Riken Japan[12] and the Trem2^{R47H} mice from Jackson Laboratories (stock #027918). Same sex littermates were group-housed (2–5 mice) with an *ad libitum* supply of food and water, under a 12-hour light/dark photoperiod, at a controlled temperature and humidity. Experiments were performed in accordance with the UK Animal (Scientific Procedures) Act, 1986 and following local ethical review. Due to the low sample size, analysis of sex differences was not performed.

METHOD DETAILS

Genotyping

Ear, tail or brain biopsy tissue was processed by either in-house UCL or Transnetyx (Cordova, TN, USA) genotyping services to determine the presence of the knock-in genes.

Tissue extraction

Animals were decapitated and the brain rapidly extracted on ice and bisected in the sagittal plane. One hemisphere was drop-fixed in 10% formalin at 4°C overnight, then transferred to a 30% sucrose, 0.02% sodium azide in phosphate-buffered saline (PBS) solution for long-term storage at 4°C. The other hemisphere was either snap frozen and processed for RNA extraction or used in other experiments not presented in the current study.

Sectioning

A portion of the dorsal cortex was removed from the formalin-fixed hemispheres, to orient the sections such that the maximal number of sections transverse to the long axis of the hippocampus could be obtained. A total of 36 serial sections containing transverse ventral-medial hippocampus were prepared at 30 μm using a frozen sledge microtome (Leica SM2010R). Sections were collected into 0.02% sodium azide in 0.1 M PBS (0.01 M phosphate buffer, 0.0027 M potassium chloride and 0.137 M sodium chloride, pH 7.4) for immunohistochemistry. A block containing the remaining mid to dorsal hippocampus was dissected out of the remaining un-sectioned tissue then paraffin-embedded and sectioned transverse to the long axis of the hippocampus at 8 μm using a rotary microtome (Leica RM2235) and collected directly onto SuperFrost plus slides for spatial transcriptomics.

Nanostring GeoMx digital spatial profiler

The paraffin embedded sections were processed by the Nanostring Technology Access Programme (Seattle, WA, USA). Epitope retrieval and staining was performed using the Leica Bond Autostainer. In the first step, the slides were baked at 60°C for 30 minutes. Heat induced epitope retrieval was then performed with 0.1 μg/ml proteinase K (Thermo Fisher, AM2546) in Epitope Retrieval Solution 2 (Leica, AR9640) for 20 minutes at 100°C. Following this, the slides were removed from the autostainer and hybridised with whole transcriptome RNA detection probes, each conjugated to a unique photocleavable DNA oligo tag (Nanostring Technologies), overnight at 37°C. Stringent washes in equal parts 4x saline-sodium citrate (SSC) buffer and 100% formamide were performed twice for 25 minutes at 37°C followed by a final wash in 2x SSC buffer. Non-specific binding was blocked using buffer W (proprietary blocking buffer from NanoString) followed by incubation with the appropriate antibodies (mouse anti-GFAP Alexa-Fluor 488 conjugate, (Invitrogen, Cat # 53-9892-82), mouse anti-Aβ40/42 Alexa Fluor 594 conjugate (Nanostring, Cat # 121301306) and rabbit anti-TMEM119 (SynapticSystems, Cat # 400 002) alongside goat anti-rabbit Alexa Fluor 647 (Thermo Fisher, Cat # A11037)). Nuclei were

counterstained (SYTO 13, Invitrogen, S7575) in buffer W for 1 hour at room temperature. Finally, the slides were washed in 2x SSC buffer.

Region of interest (ROI) selection

ROIs were defined based on the morphological stains. For each NLF and NLFTrem2^{R47H} mouse two types of ROI were defined: 1. in the region of heaviest plaque load in which all astrocytes and microglia would fall within about 30 μm of a plaque and 2. (for all genotypes), a region which did not contain plaques and with borders >50 μm from any visible plaque. One section from each mouse was used to select ROIs, with 1-3 of each type of ROI per section.

Area of interest (AOI) selection

Within the plaque containing ROI, AOIs were defined as follows:

- On plaque microglia, co-localisation of TMEM119 & Aβ42 ;
- Periplaque microglia, TMEM119 staining not colocalised with Aβ42.
- Plaque/periplaque astrocytes, all GFAP staining.

Within the ROIs without plaques, AOIs were defined as follows:

- Away microglia, all TMEM119 staining
- Away astrocytes, all GFAP staining

Library preparation and readout

RNA probe-associated DNA oligo tags were released by illuminating the chosen AOIs under ultraviolet laser exposure and aspirated into a microtiter plate, whereby each well contains the DNA oligo tags of a single AOI. The aspirates were dried and diluted in nuclease free water. DNA oligo tags were uracil removed and PCR cycled with GeoMx seq code PCR master mix (Nanostring Technologies) and GeoMx SeqCode primers (Nanostring Technologies). PCR product was AMPure bead purified initially with a 1.2x bead:sample ratio followed by a 1.2x bead:resuspended sample ratio. Samples were then sequenced on an Illumina NextSeq 2000. FASTQ files were filtered, demultiplexed, and converted to the digital count conversion file format using DND.

Analysis

Deduplicated counts were normalised to the average *Actb* and *Actg1* count as follows. For each AOI, the count for each gene was divided by the mean of the *Actb* and *Actg1* counts in that AOI and the normalised value multiplied by the mean count for *Actb* and *Actg1* across all AOIs, resulting in a normalised expression value that was comparable to the level of the raw data. Where this fell below 15 the ROI was discarded. Where >1 AOI was collected from a section for the same category (plaque, periplaque or away) the data were averaged giving n=1 per section to avoid pseudo-replication.

Histology

Free-floating 30 μm sections were washed once in PBS for 10 minutes. The sections then underwent antigen retrieval in SSC buffer (10mM, pH 9.0) for 30 minutes at 80°C. The tissues were permeabilised by washing three times for 10 minutes in 0.3% Triton X-100 in PBS (PBST). Non-specific binding was blocked for 1 hour in 10% donkey serum, followed by incubation with the appropriate primary antibodies in blocking solution at 4°C overnight (1:1000 rabbit anti-IBA1 (FujiFilm Wako Chemicals, Cat # 019-19741); 1:500 sheep anti-TREM2 (R&D Systems, Cat # AF1729); 1:500 rat anti-CD68 (Biorad, Cat # MCA1957)). The next day sections were washed three times for 10 minutes in PBST followed by a 2-hour incubation in the dark with secondary antibodies in blocking solution (1:1000 donkey anti-rabbit Alexa Fluor 594 (Invitrogen, Cat # A32754), 1:1000 donkey anti-sheep Alexa Fluor 647 (Abcam, Cat # AB150179), 1:1000 goat anti-rat Alexa Fluor 594 (Abcam, Cat # AB150160), and anti-TMEM119 as above). Finally, nuclei were counterstained with 4′,6-diamidino-2-phenylindole (DAPI) and plaques labelled with Amytracker520 (Ebba Biotech, Sweden).

Imaging for immunohistochemistry

Epiflourescent photomicrographs of whole cross-sectional hippocampal regions were serial scanned under a 20x objective at constant light, gain and exposure settings using an EVOS® FI Auto Cell imaging microscope. Three sections per animal were imaged. For all analyses, data from replicates from a single animal were averaged for n=1 estimate/animal.

CD68 epifluorescence was analysed with confocal microscopy. Images were on a Zeiss LSM 780. Z-stacks were acquired of the same tissue area and plane as plaques (20 stacks per image, 1-μm apart). DAPI was detected at a wavelength of 356 nm, CD68 at 594 nm, and Iba1 at 647 nm. Constant light intensity, gain and exposure were used for image acquisition. A minimum of 4 sections were imaged and used as a mean for each animal, and a total of 4-5 mice per group were analysed.

Protein intensity analysis

Analysis was carried out using custom written semi-automated macros within ImageJ and blinded to genotype. The macros are available at: https://doi.org/10.5281/zenodo.5847431.

- *Plaque thresholding macro*

The hippocampal region within an image was selected by manual tracing and subsequently converted to 8-bit colour and individually thresholded to account for background stain variability. The threshold for each section was established as follows:

As the Image J threshold setting is increased, the area measured decreases. By plotting a range of 40 increasing threshold settings against the associated thresholded area, as a percentage of total area, the points form an exponential decay to a 0% asymptote. When the final 40% of the values are fitted with a straight line, the intersection of this line with the data points is used for the threshold for that section. Particles <10 μm^2 were considered as noise and excluded from the analysis.

- *Plaque concentric circles macro*

For each plaque within the selected hippocampal region, concentric circles were drawn outwards with increasing 10 μm radii from the plaque, reaching a final circle with a radius of the average plaque radius plus 100 μm. Where two plaques were distanced <200 μm apart, concentric circles terminated at the nearest 10 μm to the halfway point to avoid overlapping data. As most plaques in the plaque ROIs were not more than 100 μm apart data are shown up to 50 μm from the plaque edge.

- *Concentric circles macro for controls*

For images from WT and NLFTrem2^{R47H} mice, ten randomly placed circles each with a 20 μm radius, were positioned within the hippocampus and to imitate the measurement in relation to plaques above, circles were drawn outwards with incrementing 10 μm radii reaching distance of 100 μm from the inner circle.

- *Protein intensity macro*

Fluorescence intensity within the regions identified as microglia (AU/pixels) was calculated for plaque regions and radiating concentric rings.

Microglial density analysis

Following running of the macros, microglial number (cells coexpressing IBA1 and DAPI) was manually counted for each concentric ring using Adobe Photoshop 2020 and density calculated by dividing by ring area.

QUANTIFICATION AND STATISTICAL ANALYSIS

Statistical analysis

All statistical analyses were performed using GraphPad Prism 9. Unless otherwise stated, two-way ANOVAs were followed by Sidak-corrected post hoc analyses, only in the case of a significant interaction. Statistical significance was defined as $p < 0.05$ after correction. All sample sizes represent numbers of animals; the mean of technical repeats on samples from the same animal were calculated prior to analysis. Data is plotted as mean + SEM.

ADDITIONAL RESOURCES

The genome-wide results are available at https://edwardslab.shinyapps.io/MouseacST/.